### Quench dynamics in the one-dimensional mass-imbalanced ionic Hubbard model

Zhuotao Xie, \*\* Ming Zhao, \*\* Hantao Lu, \*\* Zhongbing Huang, \*\* Gregory A. Fiete, \*\* Xiang Hu, \*\* and Liang Du <sup>1</sup>College of Physics and Technology, Guangxi Normal University, Guilin, Guangxi 541004, China <sup>2</sup>School of Physical Science and Technology & Lanzhou Center for Theoretical Physics, Key Laboratory of Theoretical Physics of Gansu Province, Lanzhou University, Lanzhou 730000, China <sup>3</sup>Department of Physics, Hubei University, Wuhan 430062, China <sup>4</sup>Department of Physics, Northeastern University, Boston, Massachusetts 02115, USA <sup>5</sup>Department of Physics, Massachusetts Institute of Technology, Cambridge, Massachusetts 02139, USA

(Received 21 November 2022; revised 20 February 2023; accepted 15 May 2023; published 24 May 2023)

Using the time-dependent Lanczos method, we study the nonequilibrium dynamics of the one-dimensional ionic-mass imbalanced Hubbard chain driven by a quantum quench of the on-site Coulomb interaction, where the system is prepared in the ground state of the Hamiltonian with a different Hubbard interaction. The exact diagonalization method (Lanczos algorithm) is adopted to study the zero temperature phase diagram in equilibrium, which is shown to be in good agreement with previous studies using density matrix renormalization group (DMRG). We then study the nonequilibrium quench dynamics of the spin and charge order parameters by fixing the initial and final Coulomb interactions while changing the quenching time protocols. Our study shows that the time evolution of the charge and spin order parameters strongly depend on the quenching time protocols. In particular, the effective temperature of the system will decrease monotonically as the quenching time is increased. By taking the final Coulomb interaction strength to be in the strong coupling regime, we find that the oscillation frequency of the charge order parameter increases monotonically with the Coulomb interaction. By contrast, the frequency of the spin order parameter decreases monotonically with increasing Coulomb interaction. We explain this result using an effective spin model and a two-site Hubbard model in the strong coupling limit. Finally, we take the final Coulomb interaction strength to be in the weak coupling regime and find that the oscillation frequency of both the charge and spin order parameters increases monotonically with decreasing Coulomb interaction. Our study suggests strategies to engineer the relaxation behavior of interacting quantum many-particle systems.

### DOI: 10.1103/PhysRevB.107.195147

### I. INTRODUCTION

The understanding of nonequilibrium dynamics of a strongly correlated electronic system has seen dramatic progress from both theoretical and experimental sides in the past decade [1-5]. Two commonly studied scenarios are the laser driven strongly correlated solid state system and a Coulomb interaction quenched system in optical lattices with cold atomic gases [3-25]. In driven systems, the observation of hidden quantum states not accessible in equilibrium [26], and the nonequilibrium control of quantum phase transitions in correlated electron systems, have attracted great interest. For example, the ac-field drive dynamical band flipping [27], the damping of Bloch oscillations in the Falicov-Kimball model [28,29] and Hubbard model [30], the ultrafast control of magnetic order in the Mott insulators [6,9,19], and photoinduced unconventional superconductivity [16,31,32] illustrate known phenomena.

In these nonequilibrium systems, the study of long-time thermalization behavior is of particular interest. In general, a closed (driven) system will thermalize to a featureless infinite temperature thermal state with maximal entropy if the energy of the system is not conserved [33-35], unless the system is sufficiently disordered for many-body localization [36,37]. If the system is coupled to a bath (i.e., "open"), it is possible to establish a nonequilibrium steady state, since the absorbed energy can be released to the connected bath [38,39]. For a clean isolated solid state system driven by spatially uniform electric field, the system could show different thermalization behavior, resulting in a featureless infinite temperature steady state, a nonthermal steady state, or even an oscillatory state [40–42]. In the case of periodic driving, the heating rate can depend on the laser frequency. Abanin et al. [43,44] find the heating rate decreases exponentially as the driving frequency is increased, provided the frequency is larger than other characteristic energy scales in the Hamiltonian. Mallayya et al. [45–47] confirm the robust exponential regime using a numerical linked-cluster expansion method, and suggest the heating rate should obey Fermi's golden rule in a weakly perturbed nonintegrable system. Seetharam et al. [13] find that the Floquet eigenstates in a clean system can exhibit nonthermal behavior because of a finite system size.

In general, a Coulomb interaction quenched system will thermalize unless the system is integrable [1,48-50]. In a

<sup>\*</sup>These authors contributed equally to this work.

<sup>†</sup>liangdu@gxnu.edu.cn

quench from a superfluid to a Mott regime, the system will thermalize in some regimes while not in others [51]. A numerical study of a finite quantum system of bosons found that the thermalization behavior depends on the magnitude of Coulomb interaction change [52] and the distance in parameter space to an integrable point, with a failure to thermalize as one approaches the integrable point [51]. By contrast, the quenched fermionic Hubbard model on an infinite dimensional Bethe-lattice system will result in a quasi-stationary state for a weak and strong Coulomb interaction quench, while in between the two regimes, a dynamical phase transition is observed, where fast thermalization occurs [53–55]. Specifically, for the SU(2) symmetry broken mass imbalanced Hubbard model, a previous Coulomb interaction quench study showed that a spin-selective (different hopping integrals) thermalization phenomena is observed [55] while studying the Coulomb interaction quench dynamics. To build the connection between the SU(2) broken (mass imbalanced) and the SU(2) preserved (mass balanced) Hubbard model, a quench of the hopping integral between the two models was studied [56]. The authors found the SU(2) symmetry order parameter decays exponentially to zero, which is character of Hubbard model.

In the equilibrium mass-balanced ionic Hubbard model, there exist rich phases: an ionic band insulator without spin order, an ionic band insulator with finite spin order, a correlated insulator, or even superconductivity [57–59]. In this work, we are interested in the one-dimensional ionic mass imbalanced Fermionic Hubbard model, which has been studied using mean-field theory (MFT) [59,60] and the density matrix renormalization group (DMRG) [61] method. Compared to the conventional Hubbard model, the translational and spin SU(2) symmetry are explicitly broken, while the mass imbalance breaks the SU(2) symmetry, the ionic term (staggered potential) breaks the translational symmetry. There exist two phases in the plane of the Coulomb interaction and the on-site ionic term for fixed mass imbalance: (i) a charge density wave order induced by the staggered ionic potential and (ii) an alternating magnetic order originating from the hopping asymmetry and Coulomb interaction. The transition at finite  $U_c$  is characterized as first order at the mean-field level [59] and second order in DMRG [61]. If one extends the above one-dimensional model to a two-dimensional square lattice, one finds novel magnetically ordered metallic phases in the Coulomb interaction and the staggered potential plane [62]. For example, a spin imbalanced ferromagnetic metal, a ferromagnetic metal, and an antiferromagnetic half metal all appear. However, the nonequilibrium behavior of this model has not been studied until now.

In this paper, we study the nonequilibrium dynamics in the one dimensional ionic Hubbard model while quenching the Coulomb interaction, where the initial state is prepared in the ground state of an initial Hamiltonian. From the technical point of view, DMRG works exceptionally well in the static case, while time-dependent DMRG suffers from significant growth of the entanglement entropy when studying quench dynamics [63–68]. In our work, we adopt the time-dependent Lanczos method in studying quench dynamics of the ionic mass imbalanced Hubbard model in one dimension.

The experimental realization of the ionic mass imbalanced Hubbard model can be implemented in ultracold atoms in engineered optical lattice systems. The hopping asymmetry (mass imbalance) can be introduced by considering two species of fermionic atoms (e.g., <sup>6</sup>Li and <sup>40</sup>K) trapped in an optical lattice [69], where the staggered ionic potential can be created by the interference of counter-propagating laser beams, and the Coulomb interaction strength can be tuned via a magnetic Feshbach resonance [70–72].

Our paper is organized as follows. In Sec. II, we describe the Hamiltonian of the one-dimensional mass imbalanced ionic Hubbard model and the time-dependent Lanczos method. In Sec. III, the equilibrium phase diagram is obtained using exact diagonalization. In Sec. IV, we calculate the nonequilibrium quench dynamics of the system in different Coulomb interaction regimes. Finally, in Sec. V, we present the main conclusions of the paper.

# II. MODEL HAMILTONIAN AND TIME-DEPENDENT LANCZOS ALGORITHM

The time dependent mass imbalanced ionic Hubbard model in one dimension is

$$H(t) = -\sum_{i\sigma} V_{\sigma}(c_{i,\sigma}^{\dagger} c_{i+1,\sigma} + c_{i+1,\sigma}^{\dagger} c_{i,\sigma}) + \Delta \sum_{i\sigma} (-1)^{i} n_{i\sigma} + U(t) \sum_{i} n_{i\uparrow} n_{i\downarrow},$$
(1)

where  $c_{i\sigma}^{\dagger}$  ( $c_{i\sigma}$ ) creates (annihilate) an electron with (pseudo) spin  $\sigma$  at site i ( $i=1,\ldots,L$ ), and  $n_{i\sigma}=c_{i\sigma}^{\dagger}c_{i\sigma}$  is the corresponding occupancy operator. Here,  $V_{\sigma}$  is the hopping integral between nearest-neighbors for spin  $\sigma$  electron,  $-\Delta$  ( $\Delta$ ) is the ionic potential for odd (even) sites of the one dimensional chain, and U(t) is the time dependent on-site Coulomb interaction.

Throughout this paper, we set  $V_{\uparrow}=1$  as the unit of energy and the time is in units of  $1/V_{\uparrow}$ , correspondingly. The hopping asymmetry (mass imbalance) is defined as the ratio of spin- $\downarrow$  to spin- $\uparrow$  hopping integrals  $\eta=V_{\downarrow}/V_{\uparrow}$ . In the following, we restrict ourselves to the half-filling case with periodic boundary conditions, where the total number of electrons N is equal to the number of sites in the chain L. Furthermore, we assume the total magnetization in the system vanishes, which means the number of up spin electrons  $N_{\uparrow}$  is equal to the down spin electrons  $N_{\downarrow}$ . The nonequilibrium quench dynamics is studied by fixing the hopping parameter  $V_{\downarrow}/V_{\uparrow} \leqslant 1$  and ionic potential  $\Delta \geqslant 0$  while quenching the Coulomb interaction from an initial  $U(t=0^-)=U_i$  to final  $U(t\geqslant t_q)=U_f$ , where  $t_q$  is the linear ramp time of Coulomb interaction change.

The exact diagonalization method (a standard Lanczos procedure) is employed to numerically find the ground state of the Hamiltonian at time  $t=0^-$  where  $U(t=0^-)=U_{\rm i}$ . This state is used as an initial state for the time dependent Schrödinger equation  $i\partial_t |\Psi(t)\rangle = H(t)|\Psi(t)\rangle$ . The time evolution is implemented step-by-step based on the time-dependent Lanczos method [73–77],

$$|\Psi(t+\delta t)\rangle \approx e^{-iH(t)\delta t}|\Psi(t)\rangle \approx \sum_{l=1}^{M} e^{-i\epsilon_l \delta t}|\Phi_l\rangle \langle \Phi_l|\Psi(t)\rangle,$$

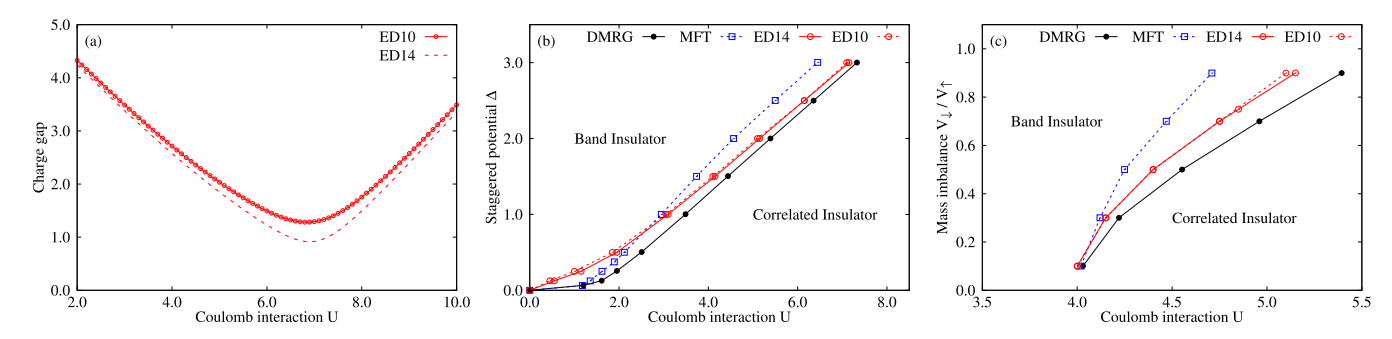


FIG. 1. The equilibrium phase diagram of the one-dimensional mass imbalanced ionic Hubbard chain at half-filling and zero temperature, calculated using the exact diagonalization method (10 sites or 14 sites with periodic boundary condition). The density matrix renormalization group (DMRG) and mean-field theory (MFT) data are obtained from the references [59,61]. (a) The charge gap  $\Delta_c$  as a function Coulomb interaction are plotted to characterize the phase transition ( $U_c = 6.8$ ), where the mass imbalance and crystal field are  $\eta = 0.75$  and  $\Delta = 3.0$ , respectively. (b) Critical points are plotted in the plane of Coulomb interaction U and crystal field  $\Delta$  with fixed mass imbalance  $\eta = V_{\downarrow}/V_{\uparrow} = 0.90$ . (c) Critical points are plotted in the plane of Coulomb interaction U and mass imbalance  $\eta$  with fixed crystal field  $\Delta = 2.0$ . The lines are guides to the eye.

(3)

where  $\epsilon_l$  ( $\Phi_l$ ) are the eigenvalues (eigenvectors) of the tri-diagonal matrix generated by Lanczos iteration with  $M \leq 100$ . (In general, the desired M for achieving the given accuracy depends on the studied setups and chosen time step sizes [78].) We set the time step size  $\delta t = 0.005$  in our calculation of the time evolution. The physical observable are computed as,

$$\langle O(t)\rangle = \langle \Psi(t)|O|\Psi(t)\rangle.$$
 (2)

Following earlier work [59], we measured the evolution of the charge and spin density order parameters,

$$\delta \rho_c(t) = -\frac{1}{L} \sum_{i\sigma} (-1)^i \langle \Psi(t) | n_{i\sigma} | \Psi(t) \rangle,$$
  
$$\delta \rho_s(t) = \frac{1}{L} \sum_{i\sigma} \sigma(-1)^i \langle \Psi(t) | n_{i\sigma} | \Psi(t) \rangle,$$

where  $\sigma = 1(-1)$  for spin- $\uparrow$  ( $\downarrow$ ) electrons in the second line. The effective temperature after Coulomb interaction quench protocol is calculated by numerically solving the equation [54]

$$E_{t \geqslant t_q} = \frac{\text{Tr}[H_{t \geqslant t_q} \exp(-\beta_{\text{eff}} H_{t \geqslant t_q})]}{\text{Tr} \exp(-\beta_{\text{eff}} H_{t \geqslant t_q})},$$
(4)

where  $E_{t\geqslant t_q}$  is the energy after the Coulomb interaction quench protocol and the effective temperature is denoted as  $T_{\rm eff}=1/\beta_{\rm eff}$ . Note here  $E_{t\geqslant t_q}$  remains constant because the time evolution operator is unitary. To solve Eq. (4) numerically, a finite temperature Lanczos algorithm [79,80] is used to calculate the total energy of the equilibrium system at finite temperature. For the analysis of long-time quench dynamics, we define the charge, spin and excitation gaps of the equilibrium Hamiltonian  $H=H_{t>t_0}$  as

$$\Delta_c = E_0(N_\uparrow + 1, N_\downarrow) + E_0(N_\uparrow - 1, N_\downarrow) - 2E_0(N_\uparrow, N_\downarrow),$$

$$\Delta_s = E_0(N_\uparrow + 1, N_\downarrow - 1) - E_0(N_\uparrow, N_\downarrow),$$

$$\Delta_E = E_1(N_\uparrow, N_\perp) - E_0(N_\uparrow, N_\perp),$$
(5)

where  $N_{\uparrow}$   $(N_{\downarrow})$  is number of the spin- $\uparrow$   $(\downarrow)$  electrons with  $N_{\uparrow} = N_{\downarrow} = L/2$ .  $E_0(N_{\uparrow}, N_{\downarrow})$  and  $E_1(N_{\uparrow}, N_{\downarrow})$  are the ground

and first excited state energy in the  $(N_{\uparrow}, N_{\downarrow})$  subspace. Note we have  $E_0(N_{\uparrow} \pm 1, N_{\downarrow}) \neq E_0(N_{\uparrow}, N_{\downarrow} \pm 1)$  due the broken SU(2) symmetry.

## III. EQUILIBRIUM PHASE DIAGRAM AT ZERO TEMPERATURE

To pave the way for the study of the nonequilibrium quench dynamics of the ionic mass imbalanced Hubbard model, we first calculate the equilibrium phase diagram using exact diagonalization (ED) and compare it with the data obtained with DMRG or MFT. In Fig. 1(a), we plot the charge gap as a function of Coulomb interaction for the one-dimensional mass imbalanced Hubbard chain with 10 or 14 sites and periodic boundary conditions. The mass imbalance and ionic potential are set as  $\eta = V_{\downarrow}/V_{\uparrow} = 0.75$  and  $\Delta = 3.0$ , respectively.

With a 10 site chain, the charge gap decreases with increasing of Coulomb interaction at first, approaching to a minimum, then increases with Coulomb interaction. As the chain size is increased from 10 to 14 sites, the charge gap as a function of Coulomb interaction takes the same characterdecreases until a critical U and then increases. With the increasing of sites, the minimum of the charge gap decreases. The corresponding Coulomb interaction with the minimum is defined as the critical Coulomb interaction  $U_c = 6.8$ . As pointed out [61], the Von Neumann block entropy can also be used as a criteria of phase transition, where the block entropy peaked at the critical Coulomb interaction U, where the charge gap dipped at the same position (shown in Appendix Fig. 8). In addition, by comparing the charge gap of 10-site and 14-site chains, we find the gap difference is smaller when the Coulomb interaction moves away from the critical value  $U_c$ , which indicates that the finite-size effect is less severe when the Coulomb interaction is away from critical  $U_c$ .

In Fig. 1(b), the phase diagram in the plane of the crystal field  $\Delta$  and Coulomb interaction U is plotted with fixed mass imbalance  $\eta = V_{\downarrow}/V_{\uparrow} = 0.9$ . The critical points are characterized by the dip of the charge gap and can be confirmed by studying the von Neumann block entropy as a function of the Coulomb interaction [61]. The band insulator and correlated insulator phase are observed in the large crystal field and

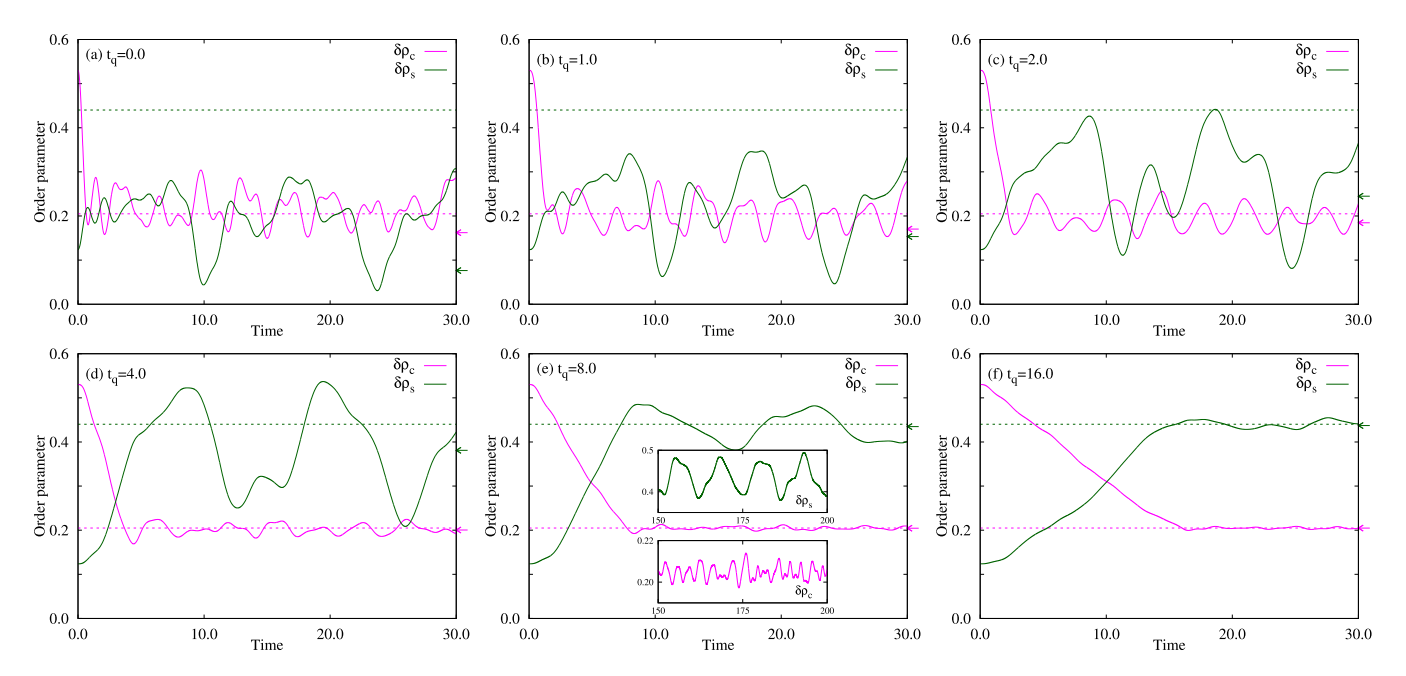


FIG. 2. Time evolution of the charge and spin order parameter  $\delta \rho_c$  and  $\delta \rho_s$  after the Coulomb interaction quench protocol  $U(t) = U_{\rm i} + (U_{\rm f} - U_{\rm i})t/t_q$  for  $t < t_q$  and  $U(t) = U_{\rm f}$  for  $t \ge t_q$ , where the initial and final Coulomb interaction strength is set as  $U_{\rm i} = 6.0$  and  $U_{\rm f} = 8.0$ , respectively. (a)  $t_q = 0.0^+$ , (b) 1.0, (c) 2.0, (d) 4.0, (e) 8.0, and (f) 16.0. The expectation value of  $\delta \rho_c$  and  $\delta \rho_s$  at zero temperature is represented by a dashed line with Coulomb interaction  $U = U_{\rm f}$  in the equilibrium calculation. The arrows indicate the thermal values of the two order parameters at effective temperature  $T_{\rm eff} = 0.632, 0.420, 0.296, 0.173, 0.104, 0.085$  for  $t_q = 0.0^+, 1.0, \ldots, 16.0$ , respectively. The insets in (e) plot the order parameters as a function of time in the long-time regime  $t \in [150, 200]$ .

large Coulomb interaction regime, respectively. To validate the exact diagonalization method used in this paper, we plot the phase diagram derived by the Hartree-Fock mean-field method and DMRG method as a comparison.

Compared to the data obtained with DMRG, exact diagonalization underestimate the critical Coulomb interaction for a fixed crystal field  $\Delta$ , which we attribute to a finite-size effect: Increasing the chain size from L=10 to 14 decreases the deviation. Furthermore, our numerical calculations show that the difference decreases with increasing  $\Delta$ . To check the dependence on the mass imbalance, the phase diagram in the plane of mass imbalance  $\eta$  and Coulomb interaction U for a fixed crystal field  $\Delta=2.0$  is plotted in Fig. 1(c). Comparing to the phase diagram calculated by DMRG, one can see that ED has worked well for large mass imbalance.

In the noninteracting limit, the charge and spin order parameter are derived analytically as  $\delta \rho_c = 0.927$  and  $\delta \rho_s =$ 0.018, respectively. With increasing Coulomb interaction, the charge order parameter  $\delta \rho_c$  will decrease while the spin order parameter  $\delta \rho_s$  increases monotonically. At specific Coulomb interaction, we have  $\delta \rho_c = \delta \rho_s$ . Further increasing the Coulomb interaction will result in  $\delta \rho_c < \delta \rho_s$  [59]. This behavior above can be understood from the two limits of the Coulomb interaction strength. In the noninteracting limit, the model can be solved analytically and the two order parameters are expressed as a function of an elliptic integral [59], where the charge order parameter increases monotonically as a function of crystal field and finally converges to  $\delta \rho_c = 1$ . Conversely, the spin order parameter will decrease monotonically and converge to 0. In the strong Coulomb interaction limit  $U \gg V_{\uparrow}, V_{\downarrow}, \Delta$ , the system will be reduced to an anisotropic XXZ Heisenberg model with a staggered magnetic field, which result in an antiferromagnetic Mott insulating phase with  $\delta \rho_s \approx 1$  and  $\delta \rho_c \approx 0$ .

The effective Hamiltonian in the strong coupling limit is [81]

$$H_{\text{eff}} = \mathcal{J}_{\text{ex}} \sum_{i} \left( S_{i}^{x} S_{i+1}^{x} + S_{i}^{y} S_{i+1}^{y} + \gamma S_{i}^{z} S_{i+1}^{z} \right) - h \sum_{i} (-1)^{i} S_{i}^{z}, \tag{6}$$

where  $S_i^{x(y,z)}$  is the spin operator at the *i*th site along direction x(y,z) and the coupling coefficients are

$$\mathcal{J}_{\text{ex}} = \frac{4UV_{\uparrow}V_{\downarrow}}{U^2 - 4\Delta^2}, \quad \gamma = \frac{V_{\uparrow}^2 + V_{\downarrow}^2}{2V_{\uparrow}V_{\downarrow}}, \quad h = \frac{4(V_{\uparrow}^2 - V_{\downarrow}^2)\Delta}{U^2 - 4\Delta^2}.$$
(7)

Here,  $\gamma \neq 1$  breaks the SU(2) symmetry and  $h \neq 0$  breaks the translational symmetry.

#### IV. NONEOUILIBRIUM OUENCH DYNAMICS

In our study of nonequilibrium quench dynamics, we fix the mass imbalance  $\eta = V_{\downarrow}/V_{\uparrow} = 0.75$  and crystal field  $\Delta = 3.0$  while changing the Coulomb interaction strength U(t). The quench protocol is defined through the time dependent Coulomb interaction as

$$U(t) = \begin{cases} U_{i} + \alpha t & t < t_{q} \\ U_{f}, & t \geqslant t_{q} \end{cases}$$
 (8)

where  $\alpha = (U_f - U_i)/t_q$  is the slope of ramp in the Coulomb quench protocol. The starting state is set as the ground state of the initial equilibrium Hamiltonian with  $U(t = 0^-) = U_i$ .

TABLE I. Effective temperatures in the long-time limit for quench protocols (8) with different quench time  $t_q$  are summarized, where the initial and final Coulomb interaction are fixed as  $U_{\rm i}=6.0$  and  $U_{\rm f}=8.0$ . Here,  $\delta\rho_c(T_{\rm eff})$  and  $\delta\rho_c(T_{\rm eff})$  are the charge and spin order parameters in the equilibrium calculation with  $U=U_{\rm f}$  and  $T=T_{\rm eff}$ , respectively.  $\delta\bar{\rho}_c$  and  $\delta\bar{\rho}_s$  are the long-time ( $t\in[150,200]$ , not shown in Fig. 2) averaged charge and spin order parameters from the nonequilibrium quench dynamics calculation.

$t_q$	$T_{ m eff}$	$\delta ho_c^{th}$	$\deltaar ho_c$	$\delta  ho_s^{th}$	$\deltaar ho_s$
0.0	0.632	0.1622	0.2197	0.0763	0.1916
1.0	0.420	0.1703	0.2077	0.1534	0.2356
2.0	0.296	0.1847	0.2026	0.2449	0.2934
4.0	0.173	0.2005	0.2024	0.3810	0.3891
8.0	0.104	0.2045	0.2047	0.4348	0.4346
16.0	0.085	0.2048	0.2049	0.4372	0.4397

The time evolution of the initial state is based on the time-dependent Hamiltonian in Eq. (1).

# A. Nonequilibrium quench dynamics: dependence on ramp time in the quench protocol

To study the dependence of the ramp time in the quench protocol, we fix the initial and final Coulomb interaction  $U_i$ ,  $U_f$  while changing the quench time  $t_q$ . In our calculation, we set the initial and final Coulomb interaction as  $U_i = 6.0$  and  $U_f = 8.0$ , where the critical interaction between band and correlated insulator is  $U_c = 6.8$ . In Fig. 2, we plot the nonequilibrium evolution of the charge and spin order parameters in the Hamiltonian, Eq. (1), with different quench time  $t_q = 0.0^+$ , 1.0, 2.0, 4.0, 8.0, 16.0. The zero temperature ground state expectation values of  $\delta \rho_c$  and  $\delta \rho_s$  in equilibrium with Coulomb interaction  $U = U_f$  are represented with dashed line  $\delta \rho_c = 0.205$  and  $\delta \rho_s = 0.440$ . The initial order parameters in equilibrium (t = 0) are  $\delta \rho_c(t = 0) = 0.530$  and  $\delta \rho_s(t = 0) = 0.124$ , respectively.

In the case with quench time  $t_q = 0.0^+$  in Fig. 2(a) (the quench protocol is defined via a Heaviside step function), the two order parameters are intertwined with each other. The charge order parameter as a function of time oscillates around  $\delta \bar{\rho}_c = 0.2197$  (long-time averaged value), which is close to the equilibrium value at zero temperature,  $\delta \rho_c^{eq} = 0.205$ . By contrast, the spin order parameter oscillates about  $\delta \bar{\rho}_s = 0.1916$ , which is far from the equilibrium value at

zero temperature  $\delta \rho_s^{eq} = 0.440$ . By using the definition of effective temperature Eq. (4), we find  $T_{\rm eff} = 0.632$ . If the equilibrium calculation is done with  $U = U_{\rm f}$  at temperature  $T = T_{\rm eff} = 0.632$ , we have the charge and spin order parameter at the thermalized state  $\delta \rho_c^{th} = 0.1622$  and  $\delta \rho_s^{th} = 0.0763$ , which are represented as arrows in the plot. By defining the oscillating amplitude as the difference between the maximum and the minimum of the order parameter after t > 20, we find the amplitude of charge order parameter is about  $A(\delta \rho_c) = 0.092$ , which is smaller than the spin order parameter  $A(\delta \rho_s) = 0.241$ .

In Fig. 2(b), we plot the time evolution of the two order parameters with a different quench time,  $t_q = 1.0$ . In the quenching time regime  $t < t_q$ , a monotonically increasing (decreasing) behavior of spin order (charge order) parameter is observed. Compared to the case with  $t_q = 0.0^+$ , the oscillation amplitude of the spin and charge order parameter are larger with  $A(\delta \rho_c) = 0.134$  and  $A(\delta \rho_s) \approx 0.283$ . The effective temperature is  $T_{\rm eff} = 0.420$ . The order parameters at the effective temperature are  $\delta \rho_c^{th} = 0.1703$  and  $\delta \rho_s^{th} = 0.1534$ , and are indicated by the arrows on the right side of the figure. In Figs. 2(c)-2(f), the quench protocol is changed by increasing the quenching time as  $t_q = 2.0$ , 4.0, 8.0, and 16.0. Upon further increasing the quench time, the oscillation amplitude will decrease and the oscillation center (long-time averaged value) moves closer to the one with zero temperature in equilibrium. The calculated effective temperatures are  $T_{\rm eff} = 0.296, 0.173, 0.104, \text{ and } 0.085, \text{ from which we con-}$ clude that the effective temperature decreases with increasing quench time,  $t_a$ .

Finally, we summarize the values of  $T_{\rm eff}$ ,  $\delta \bar{\rho}_c$ ,  $\delta \bar{\rho}_s$  and  $\delta \rho_c^{th}$ ,  $\delta \rho_s^{th}$  for different quench times  $t_q$  in Table I. From the table, we find that the charge order parameter slightly changes with temperature, while the spin order parameter changes significantly. The phenomenon can be understood by calculating the charge gap  $\Delta_c = 1.7547$  and spin gap  $\Delta_s = 0.4132$  of the system, where the corresponding changes are smaller for a larger gap. Furthermore, the thermalized value of the charge and spin order parameters are equal to the long-time averaged value in nonequilibrium, only when the  $t_q \geqslant 4.0$ .

The systematic quench time behavior can be understood as longer quench times  $t_q$  making the Hubbard U increase closer to an adiabatic evolution, and therefore inducing less heating. By checking the difference of the thermal values (arrows) and the expectation values at zero temperature (dashed line), we

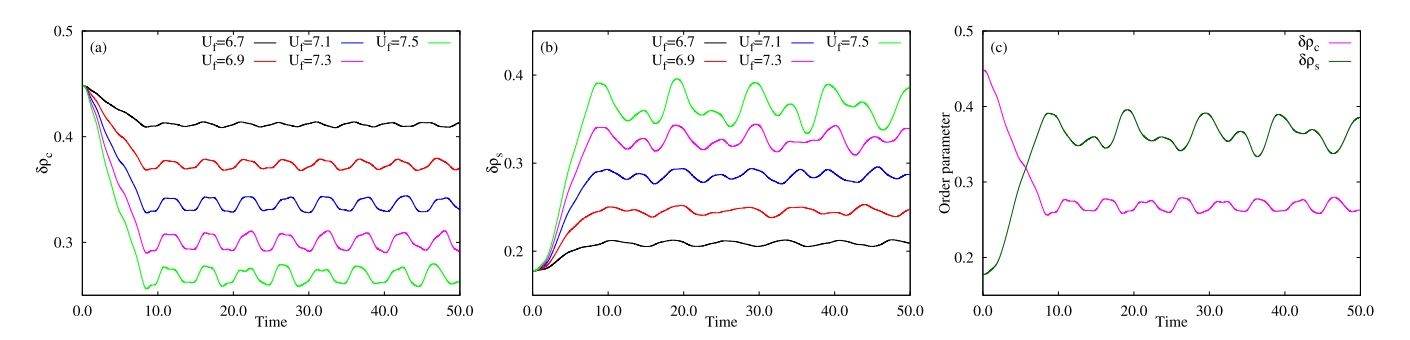


FIG. 3. Time evolution of charge and spin order parameter  $\delta \rho_c$  (a) and  $\delta \rho_s$  (b) for Coulomb quenches from  $U_i = 6.5$  to  $U_f = 6.7, 6.9, \dots, 7.5$ , (c) Comparison of  $\delta \rho_c$  and  $\delta \rho_s$  for quench from  $U_i = 6.5$  to  $U_f = 7.5$ .

TABLE II. Oscillation amplitude of the charge and spin order parameters for quench protocols with different final  $U_{\rm f}$ . The ramp time  $t_a$  and initial interaction value  $U_{\rm i}$  are kept fixed.

$t_q$	$U_{ m i}$	$U_{ m f}$	$A(\delta  ho_c)$	$A(\delta  ho_s)$
8.0	6.5	6.7	0.005	0.007
8.0	6.5	6.9	0.010	0.010
8.0	6.5	7.1	0.013	0.014
8.0	6.5	7.3	0.017	0.031
8.0	6.5	7.5	0.021	0.058

find that the spin order parameter  $\delta \rho_s$  is much more sensitive to the effective temperature (greater for smaller  $t_q$ ) than the charge order parameter  $\delta \rho_c$ .

# **B.** Nonequilibrium quench dynamics near the critical Coulomb interaction

For the case with mass imbalance  $\eta = V_{\downarrow}/V_{\uparrow} = 0.75$  and crystal field  $\Delta = 3.0$ , the critical Coulomb interaction is  $U_c = 6.8$  for the transition from band insulator to correlated insulator in equilibrium. To investigate the quench dynamics around the critical Coulomb interaction, we set the initial Coulomb interaction as  $U_{\rm i} = 6.5$  and the final Coulomb interaction to be near the critical value,  $U_c = 6.8$ . The quenching time is fixed at  $t_q = 8.0$  while the slope for the quench protocol is  $(U_{\rm f} - U_{\rm i})/t_q$  is different for each specific  $U_{\rm f}$ .

In Figs. 3(a) and 3(b), we plot the time evolution of the charge and spin order parameters after a Coulomb interaction quench from  $U_i = 6.5$  to different  $U_f = 6.7$ , 6.9, 7.1, 7.3, and 7.5. The charge and spin order parameters are  $\delta \rho_c = 0.448$  and  $\delta \rho_s = 0.178$  for the initially prepared equilibrium system with  $U_i = 6.5$ . In the time range  $0 < t < t_q$ , the charge (spin) order parameter decreases (increases) monotonically, which can be attributed to the increase of the Coulomb interaction. Over the time range  $t > t_q$ , the two order parameters oscillate with different amplitudes. The amplitudes are summarized in Table II, which are 0.005, 0.010, 0.013, 0.017, and 0.021 for charge order parameters and 0.007, 0.010, 0.014, 0.031, and 0.058 for spin order parameters. To compare the two order parameters, we plot the two in Fig. 3(c) with a final Coulomb interaction of  $U_f = 7.5$ .

The only crossing of the two order parameters is observed at time  $t \approx 5.69$ , followed by approximately periodic oscillation.

### C. Nonequilibrium quench dynamics: quench from weak to strong Coulomb interaction limit

In order to observe the oscillating behavior clearly, we set the final Coulomb interaction deep in the strong interaction regime. In Fig. 4(a), we plot the charge and spin order parameter for the Coulomb interaction quench from  $U_i = 2.0$ ,  $U_f = 8.0$ . In the region  $t > t_q$ , the charge order parameter is oscillating around its equilibrium value  $\delta \rho_c = 0.205$ , while the spin order parameter is oscillating around  $\delta \bar{\rho}_s = 0.330$ , which deviate from its equilibrium value at zero temperature  $\delta \rho_s = 0.438$ . The effective temperature at  $t \ge t_q$  is  $T_{\rm eff} = 0.215$ , where the order parameters are  $\delta \rho_c^{th} = 0.201$  and  $\delta \rho_s^{th} = 0.385$ .

To illustrate the behavior of the charge and spin order parameters in the strong Coulomb interaction regime following a quench, we plot the spin-order parameter for the Coulomb interactions  $U_{\rm f}=8.0,\ 12.0,\ 16.0,\ {\rm and}\ 20.0$  while fixing the initial Coulomb interaction as  $U_{\rm i}=2.0$  in Figs. 4(b) and 4(c). Apparently, the oscillation frequency of the charge order parameter increases monotonically with Coulomb interaction  $U_{\rm f}$ . Conversely, the oscillation frequency of the spin order parameter decrease with the Coulomb interaction. We have checked that the oscillating frequency for both charge and spin order are independent of initial Coulomb interaction  $U_i$  and quenching time  $t_a$  (shown in Appendix Fig. 7).

For the time evolution of the spin order parameter, it can be understood in the strong Coulomb interaction limit, where the effective Hamiltonian can be approximately described as an anisotropic XXZ spin model. In the effective spin Hamiltonian, the behavior is dominated by the spin excitation with energy scale  $\mathcal{J}_{\rm ex}$  defined in Eq. (7), which is in agreement with previous experiments [82]. The effective Hamiltonian, Eq. (7), is an XXZ model with exchange coupling  $\mathcal{J}_{\rm ex}$ . For the final Coulomb interaction  $U_{\rm f}=12.0, 14.0, 16.0, \text{ and } 20.0, \text{ the corresponding exchange interaction are } \mathcal{J}_{\rm ex}=0.333, 0.263, 0.218, \text{ and } 0.165, \text{ respectively.}$  The oscillation periods of the charge density order parameter are 3.27, 1.15, 0.69, and 0.50 for  $U_{\rm f}=1.00$ 

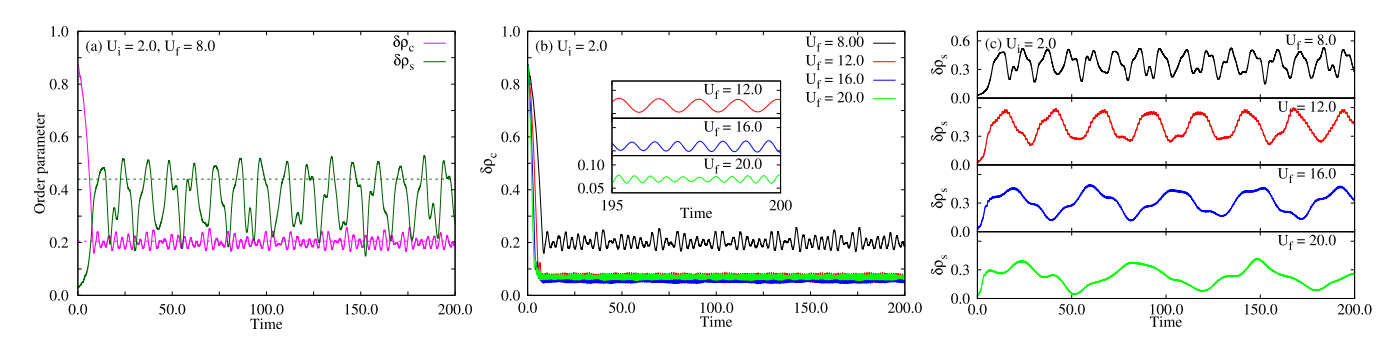


FIG. 4. Time evolution of the charge and spin order parameters  $\delta \rho_c$  and  $\delta \rho_s$  for the quench protocol with (a)  $U_{\rm i} = 2.0 \rightarrow U_{\rm f} = 8.0$ , where the quench time  $t_q = 8.0$ . The dashed line represents the equilibrium  $\delta \rho_c$  and  $\delta \rho_s$  at zero temperature with  $U = U_{\rm f}$ . (b)  $U_{\rm i} = 2.0 \rightarrow U_{\rm f} = 8.0$ , 12.0, 16.0, and 20.0, and the periods of the charge density order parameter are 3.27, 1.15, 0.69, and 0.50. The inset shows the oscillation behavior at 195 < t < 200 for  $U_{\rm f} = 12$ , 16, and 20. (c)  $U_{\rm i} = 2.0 \rightarrow U_{\rm f} = 8.0$ , 12.0, 16.0, and 20.0, and the periods of the spin density order parameter are 12.40, 24.32, 43.72, and 63.53.

TABLE III. Oscillation periods of the charge and spin order parameters ( $T^c$  and  $T^s$ ) in the long-time limit for quench protocols (8) with quench time  $t_q = 8.0$ . The initial Coulomb interaction is fixed as  $U_i = 6.0$ . Here,  $\Delta_s$ ,  $\Delta_c$ ,  $\Delta_E$  are the spin, charge and excitation gaps [Eq. (5)] for the equilibrium Hamiltonian with  $U = U_f$ .

$U_{ m f}$	$2\pi/T^c$	$2\pi/T^s$	$\Delta_s$	$\Delta_c$	$\Delta_E$
8.0	1.9205	0.5065	0.4132	1.7547	0.5144
12.0	5.4609	0.2582	0.1892	5.4069	0.2428
16.0	9.1014	0.1436	0.1000	9.3305	0.1450
20.0	12.560	0.0958	0.0852	13.2892	0.0927

8.0, 12.0, 16.0, and 20.0. The periods of the spin density order parameter are 12.40, 24.32, 43.72, and 63.53, which increase monotonically with Coulomb interaction.

Furthermore, to understand the origin of the behavior with increasing  $U_f$ , one can consider a two-site Hubbard model at half-filling in the strong Coulomb interaction limit, where the hopping terms are considered as a perturbation. The energy levels from lowest to highest are the singly occupied singlet and triplet, and the other two energy levels have a double occupancy on one of the sites. The oscillations of the spin order parameter will be determined mainly by the excitation energy between the singlet and the triplet, which is the effective Hund's coupling energy,  $\mathcal{J}_{\rm ex} \sim U^{-1}$ . By contrast, the oscillations of the charge order will incorporate the excitation between singly occupied and doubly occupied states, where the energy difference will be mainly determined by Coulomb interaction U. This explains the corresponding monotonically decreasing and increasing oscillation period trends of the charge and spin order parameters with increasing  $U_{\rm f}$ .

Finally, to qualitatively understand the oscillating behavior above, we numerically calculate the charge, spin and excitation gaps [Eq. (5)] for the equilibrium Hamiltonian with  $U = U_{\rm f}$ . For the strong Coulomb interaction limit ( $U_{\rm f} = 20.0$ , for example), the oscillation frequency of charge order is 12.56, which is close to the charge gap 12.2892, and the oscillation frequency of spin order is 0.0958, which is close to the excitation gap 0.0927. Similar behaviors are observed for  $U_{\rm f} = 16.0$ , 12.0, and 8.0, which suggest that energetically low-lying states are dominating the nonequilibrium dynamics. The equilibrium spin, charge, and excitation gaps at different Coulomb interaction  $U_{\rm f}$  are summarized in Table III.

## D. Nonequilibrium quench dynamics: quench from strong to weak Coulomb interaction

In the previous section, we calculated the quench dynamics while quenching the Coulomb interaction from the weak to the strong coupling regime, and we found that the oscillation frequency is dependent on the charge gap (charge order parameter) and the excitation gap (spin order parameter). To check the generality of the conclusions obtained above, we study the quench dynamics from a different direction in this subsection–from the strong coupling regime to the weak Coulomb interaction region.

In Fig. 5, we plot the time evolution of the charge and spin order parameters, while quenching the Coulomb interaction from  $U_{\rm i}=12.0$  to  $U_{\rm f}=8.0, 6.0, 4.0$  with fixed quenching time  $t_q=8.0$ . The initial state is the ground state of the equilibrium Hamiltonian with  $U_{\rm i}=12.0$ , where the charge and spin order parameters are  $\delta\rho_c=0.0465$  and  $\delta\rho_s=0.5528$ . For the quenching from  $U_{\rm i}=12.0$  to  $U_{\rm f}=8.0$  [Fig. 5(a)], this is an in phase (Mott phase) quench. The time evolution monotonically increase (decrease) for spin (charge) order parameters, followed by an oscillation.

Focusing on the long-time oscillation behavior, the approximate oscillation frequency of charge and spin order parameter are  $\omega_c=2\pi/T^c=1.8845$  ( $T^c=3.3325$ ) and  $\omega_s=2\pi/T^s=0.5050$  ( $T^s=12.4344$ ), respectively. The excitation, charge and spin gaps for U=8.0 are  $\Delta_E=0.5144$ ,  $\Delta_c=1.7547$  and  $\Delta_s=0.4132$ , respectively. Upon decreasing the final Coulomb interaction to  $U_{\rm f}=6.0,4.0$ , a crossing point is observed at short times, followed by oscillating parameters. The oscillation of the spin order parameters is clear, while the oscillation behavior of the charge order parameter is irregular.

By comparing the long-time oscillation of charge and spin order, the oscillation of charge is approximately the same frequency as the spin order. This can be explained because the equilibrium charge gap and excitation gap are approximately equal to each other. The oscillating frequency for  $U_i = 12.0 \rightarrow U_f = 6.0$  is  $\omega_s = 2\pi/T^s = 1.2182$  ( $T^s = 5.1550$ ). The excitation, charge and spin gaps are  $\Delta_E = 1.2265$ ,  $\Delta_c = 1.4926$ , and  $\Delta_s = 1.2282$ , respectively. The oscillating frequency for  $U_i = 12.0 \rightarrow U_f = 4.0$  is  $\omega_s = 2.6556$  ( $T^s = 2.3660$ ). The excitation, charge and spin gaps are  $\Delta_E = 2.6511$ ,  $\Delta_c = 2.6645$ , and  $\Delta_s = 2.7137$ , respectively.

In summary, with decreasing the final Coulomb interaction in the band insulating region, we find that both the charge

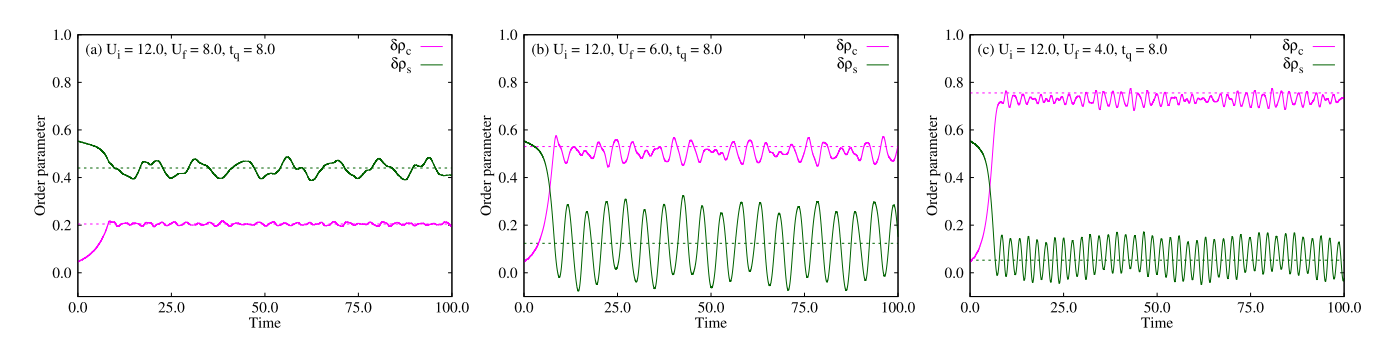


FIG. 5. Time evolution of charge and spin order parameter  $\delta \rho_c$  and  $\delta \rho_s$  for Coulomb quenches from  $U_i = 12.0$  to  $U_f = 8.0$ , 6.0, and 4.0. This goes from strong coupling to weak coupling.

and spin order oscillation decrease, and the frequency of the two are very close to each other. This can be explained by the charge and the excitation gap of the final Hamiltonian.

### V. CONCLUSION

In this paper, the exact diagonalization (time dependent Lanczos) method is used to study the quench dynamics in the one-dimensional ionized Hubbard model with mass imbalance. To check the validity of ED used in studying the system, we first studied the phase diagram in equilibrium and compared it with the phase diagram calculated using DMRG and Hartree-Fock mean-field methods. Qualitatively, the ED calculation shows that the transition between the band insulator and correlated insulator is of second order, which is consistent with DMRG calculations.

The phase diagram in the Coulomb interaction and crystal field plane U- $\Delta$  is studied. The critical Coulomb interaction deviate from the DMRG result for a small  $\Delta < 0.25$  region. The phase diagram in the U- $\eta$  plane ( $\eta$  is mass imbalance) is studied. In comparison with DMRG, we find ED works well for relative large mass imbalance  $\eta \leq 0.75$ . Furthermore, finite-size effects are studied by considering 10-site and 14-site chains. We find that increasing the number of sites will slightly improve the agreement with DMRG. In the nonequilibrium quench dynamics study we choose the mass imbalance and the crystal field parameters as  $\eta = 0.75$  and  $\Delta = 3.0$  in this paper, respectively, where the phase transition point from band insulator to correlated insulator is  $U_c = 6.8$  in equilibrium.

Focusing on the nonequilibrium evolution after a Coulomb quench, we study the dependence on the quenching time  $t_q$  for a fixed initial and final Coulomb interaction  $U_i = 6.0$  and  $U_f = 8.0$ , where  $U_i = 6.0$  is in the band insulating regime in equilibrium and  $U_f$  is situated in the correlated insulating regime. By inspecting the time evolution of the charge and spin order parameters, we observe that the two order parameters exhibit different oscillation behaviors, which depend on the quenching time. In general, a monotonically increasing (decreasing) spin (charge) order parameter at short times followed by an approximate oscillating behavior at long-times is observed.

In the long-time regime, the order parameters oscillate around their thermalized equilibrium value, where an effective temperature is defined. Furthermore, the effective temperature will decrease monotonically with quenching time for fixed initial and final Coulomb interaction  $U_i$  and  $U_f$ , where an approximate adiabatic evolution is observed for very large  $t_a$ .

Finally, we study the nonequilibrium time evolution in the parameter regime where  $U_i$  is in the band insulation region and  $U_{\rm f}$  is deep in the correlated insulating region (as well as the opposite initial and final interaction values). We find that the spin and charge order parameters will oscillate with time in the long-time regime. The oscillation frequency in the long-time regime depends only on the final Hamiltonian, and is independent of the quenching time in the protocol or the initial Hamiltonian. When the final Hamiltonian is in the correlated insulating regime, the oscillation frequency of the charge (spin) order parameter will increase (decrease) monotonically with increasing Coulomb interaction. By contrast, when the final Hamiltonian is in the band insulating regime, the oscillating frequency of the charge and spin order parameter will both increase monotonically with decreasing Coulomb interaction. The observed oscillation behaviors are quantitatively explained with the charge and excitation gaps of the final Hamiltonian.

In summary, we studied the nonequilibrium time evolution of the mass imbalanced ionic Hubbard model driven by a Coulomb interaction quench. Our results show that the dynamical evolution of physical observables exhibit different behaviors depending on the quench protocol, where the effective temperature decreases with increasing quench time. When the final Coulomb interaction strength is situated deep in the correlated regime, the oscillation period of the spin (charge) order parameter will increase (decrease) monotonically with Coulomb interaction strength, which is independent of quench protocol. Furthermore, when the final Coulomb interaction strength is situated deep in the band insulating regime, the oscillation frequency of the spin and charge order parameter will both increase monotonically with decreasing Coulomb interaction strength. Our results can be tested experimentally in cold atom optical lattices, and may offer strategies to engineer the relaxation behavior of interacting quantum many-particle systems.

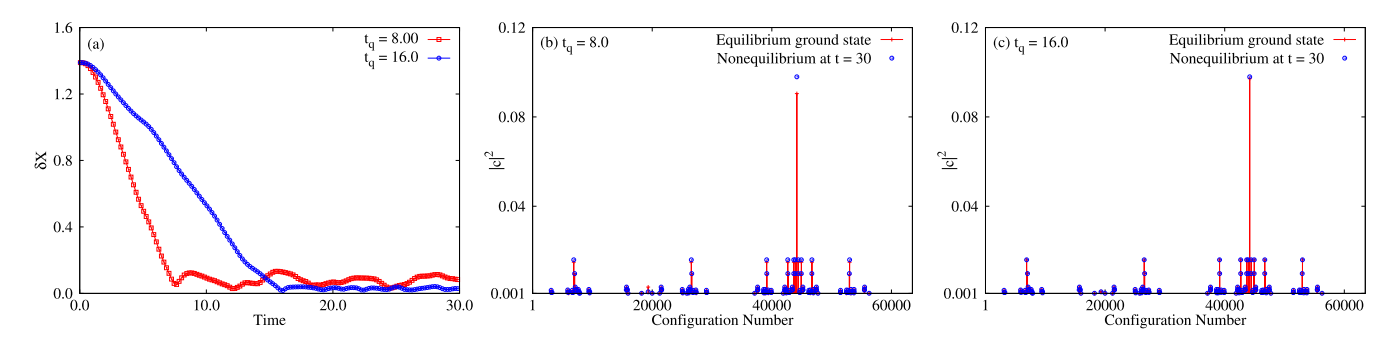
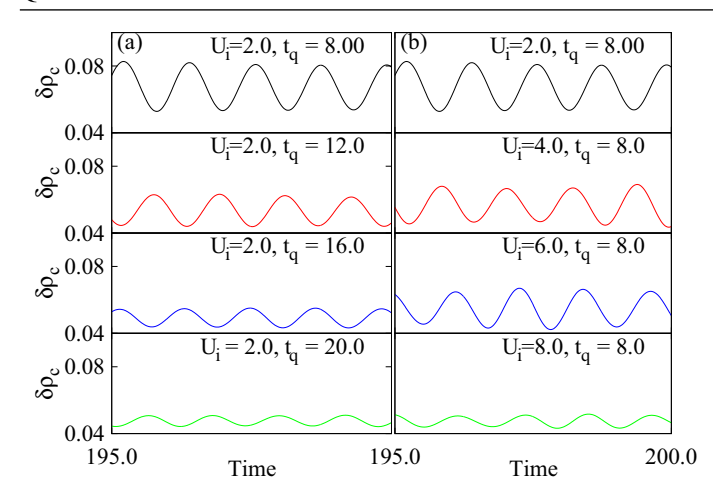


FIG. 6. The initial and final Coulomb interaction are fixed as  $U_i = 6.0$  and  $U_f = 8.0$ . (a) The time evolution of  $\delta X$  in Eq. (A1) are plotted as a function of time with the quenching time  $t_q = 8.0$  and  $t_q = 16.0$ , respectively. [(b) and (c)] The probability distribution of each Fock basis for  $|c_I|^2 = |\langle I|\Psi_g^f\rangle|^2$  and  $|\langle I|\Psi(t)\rangle|^2$  are plotted with quenching time  $t_q = 8.0$  (b) and  $t_q = 16.0$  (c), respectively, where  $|\Psi_g^f\rangle$  is the ground state of equilibrium Hamiltonian with  $U = U_f$ ,  $|\Psi(t)\rangle$  is the time evolved wave function from nonequilibrium time evolution.



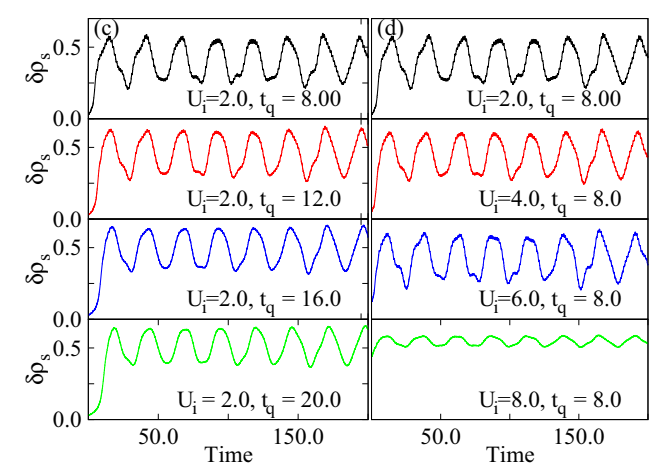


FIG. 7. Time evolution of the charge (a) and spin (c) order parameter  $\delta \rho_c$  and  $\delta \rho_s$  after the Coulomb interaction quench where the initial and final Coulomb interactions are set as  $U_i = 2.0$  and  $U_f = 12.0$ , respectively. The quench protocols with different quenching time  $t_q = 8.0$ , 12.0, 16.0, and 20.0 are applied, respectively. Time evolution of  $\delta \rho_c$  (b) and  $\delta \rho_s$  (d) for different quench protocols with fixed final Coulomb interaction  $U_f = 12.0$  and quenching time  $t_q = 8$  while the initial Coulomb interaction is changed with  $U_i = 2.0$ , 4.0, 6.0, and 8.0.

#### ACKNOWLEDGMENTS

We acknowledge helpful discussions with Xiaojun Zheng, Huan Li, Yun Guo, and Xiaojun Sun. We gratefully acknowledge funding from the National Natural Science Foundation of China (Grant No. 11904143, No. 12174168, No. 12047501, No. 12147211, and No. 12065002), the Natural Science Foundation of Guangxi Province Grant No. 2020GXNS-FAA297083, GuiKe AD20297045. G.A.F. gratefully acknowledges funding from US National Science Foundation grant DMR-2114825 and the Alexander von Humboldt Foundation.

# APPENDIX A: THE EFFECT OF LONG QUENCHING TIME ON THE SYSTEM STATE

The time evolution of the ground state wave function that approximates adiabatic evolution under a long quenching time is studied here. In Figs. 2(e) and 2(f), the quenching time in protocols are  $t_q = 8.0$  and  $t_q = 16.0$ , respectively. The effective temperature of the systems are  $T_{\rm eff} = 0.104$ , 0.085 (close to 0 K), where the nonequilibrium ramp process can possibly be approximated as an adiabatic process.

To characterize the difference between the nonequilibrium evolution studied in our work and an adiabatic process, we define a parameter  $\delta X$  to measure the difference between the time evolved wave function and the ground state of equilibrium Hamiltonian at  $H_{t \geq t_0}$ ,

$$\delta X(t) = \sum_{I} \left| \langle \Psi(t) | I \rangle \langle I | \Psi(t) \rangle - \left\langle \Psi_{g}^{f} \left| I \rangle \langle I \middle| \Psi_{g}^{f} \right\rangle \right|, \quad (A1)$$

where  $|\Psi_g^f\rangle$  is the equilibrium ground state wave function of the final Hamiltonian with  $U=U_{\rm f}, |\Psi(t)\rangle$  corresponds to nonequilibrium wave function at time t, and I labels the i-th Fock basis state in the many-body Hilbert space.

In Fig. 6(a), the parameter  $\delta X$  with quenching times  $t_q = 8.0$  and 16.0 are plotted as a function of time. It is observed that the parameter  $\delta X$  decreases monotonically and tends to approach 0. To further understand the detailed difference between the two wave functions, we plot the probabilities of each Fock basis state in Figs. 6(b) and 6(c) for the equilibrium wave function  $|\langle I|\Psi_g^f\rangle|^2$  and the nonequilibrium wave function  $|\langle I|\Psi(t)\rangle|^2$  at t=30 with different quenching times  $t_q=8.0$  and  $t_q=16.0$ , respectively. we find the basis with highest probability is  $|\downarrow,\uparrow,\downarrow,\uparrow,\cdots,\downarrow,\uparrow\rangle$ . By comparing the time evolved wave function and the ground state of equilibrium Hamiltonian at  $H_{t\geqslant t_q}$ , we conclude that the time evolution of ground state in initial Hamiltonian will converge

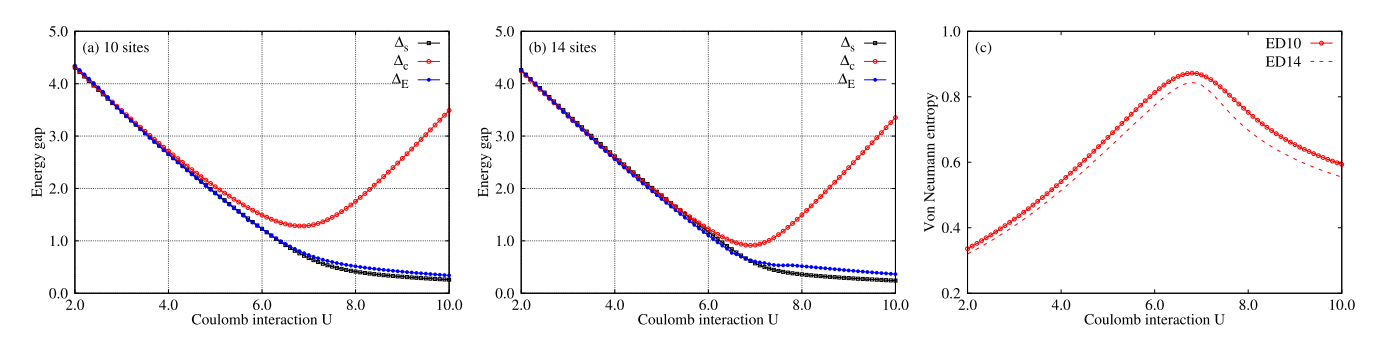


FIG. 8. [(a) and (b)] The charge, spin and excitation gap of the ionic mass imbalanced Hubbard model as a function Coulomb interaction U. The mass imbalance and the ionic potential are  $\eta=0.75$  and  $\Delta=3.00$ . The calculation is done with 10 and 14 sites, respectively. (c) The Von Neumann block entropy as a function of Coulomb interaction is plotted.

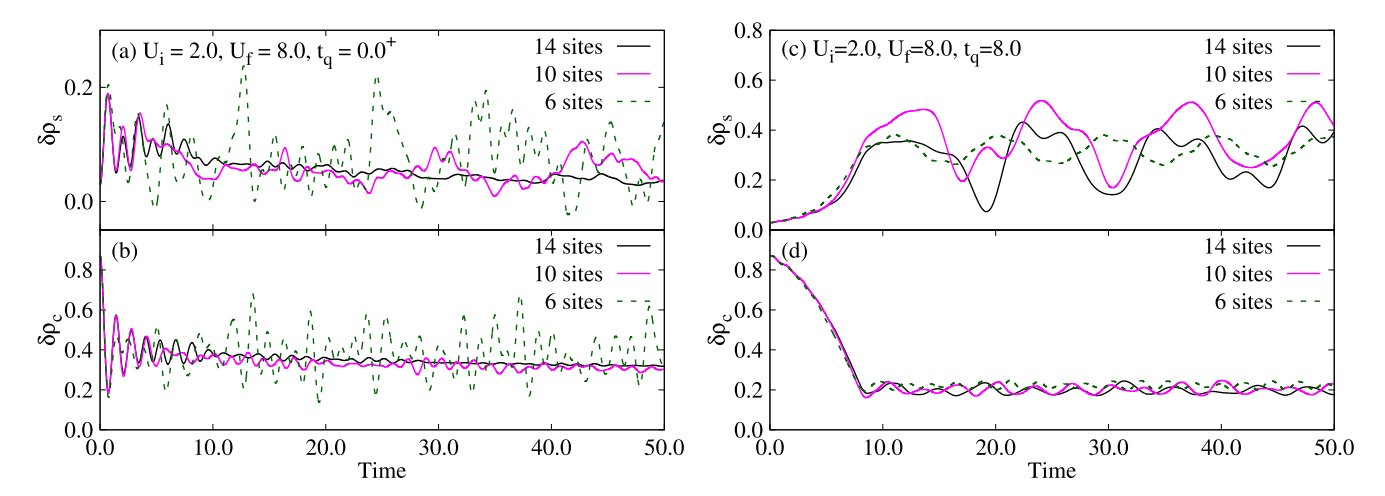


FIG. 9. Time evolution of the charge and spin order parameter  $\delta \rho_c$  and  $\delta \rho_s$  after the Coulomb interaction quench where the initial and final Coulomb interactions are set as  $U_i = 2.0$  and  $U_f = 8.0$ , respectively. The quenching time is fixed at  $t_q = 0.0$  [(a) and (b)] and 8.0 [(c) and (d)]. The order parameters are calculated with 6, 10, and 14 sites with periodic boundary condition, respectively.

to the ground state of the final Hamiltonian  $H_{t\geqslant t_q}$ , for long quenching time.

# APPENDIX B: EFFECTS OF QUENCHING TIME AND INITIAL COULOMB INTERACTION ON THE OSCILLATION PERIOD OF THE ORDER PARAMETER

Here we study the effect of quenching time  $t_q$  on the oscillation period of the order parameter of the system under strong interactions. By setting the initial and final Coulomb interaction as  $U_{\rm i}=2.0$  and  $U_{\rm f}=12.0$ , we plot the time evolution of the charge and spin order parameters with different quenching times  $t_q=8.0,\ 12.0,\ 16.0,\$ and 20.0 in Figs. 7(a) and 7(c). By solving Eq. (4), the effective temperatures are  $T_{\rm eff}=0.345,\ 0.114,\ 0.089,\$ and 0.020, respectively. The oscillation period of the charge density and spin order parameters are  $T^c\approx 1.16$  and  $T^s\approx 26.02$ , which are independent of the quenching time.

In addition, we study the oscillation behavior of the charge and spin order parameters by fixing the final Coulomb interaction  $U_{\rm f}=12.0$  in the strong Coulomb interaction regime with quenching time  $t_q=8.0$  while changing the initial Coulomb interaction  $U_{\rm i}=2.0,~4.0,~6.0,~{\rm and}~8.0$ . The two order parameters as a function of time are plotted in Figs. 7(b) and 7(d). Our numerical results show that the oscillation periods of the charge density and spin density order parameters are about  $T^c\approx1.15$  and  $T^s\approx24.03$ , which are independent of the initial Coulomb interaction strength.

### APPENDIX C: FINITE-SIZE EFFECTS

To check the finite-size effects in the equilibrium study of the mass imbalanced ionic Hubbard model, we calculate the charge, spin and excitation gap of the system for different Coulomb interactions U. The mass imbalance is  $\eta=0.75$ , the ionic potential is  $\Delta=3.0$ . We perform the calculation with 10 sites [Fig. 8(a)] and 14 [Fig. 8(b)] sites as a comparison. As suggested in previous works, the Von Neumann entropy can be adopted as a criteria for distinguishing the phase boundary of a quantum phase transition, where the transition occurs when the entropy is peaked [61]. The Von Neumann block entropy is defined as  $S_A=-{\rm Tr}\varrho_A \ln \varrho_B$ , where A, B is the block including the first and second half of the chain sites.  $\varrho_A={\rm Tr}_B\varrho$  is the partial trace with  $\varrho=|\Psi_g\rangle\langle\Psi_g|$ . From the plot of Von Neumann entropy as a function of Coulomb interaction in Fig. 8(c), we find that except the quantitative difference between the calculated values with 10 and 14 sites, the peaked position is approximately the same.

In studying the nonequilibrium quench dynamics, we calculate the time evolution of the charge and spin order parameters with 10 sites (Fig. 9), as a comparison with 6 or 14 sites (within our calculation ability). The initial and final Coulomb interactions are set as  $U_i = 2.0$  and  $U_f = 8.0$ with fixed quench time  $t_q = 0.0^+$  [(a) and (b)] and 8.0 [(c) and (d)]. In the  $t_q = 0.0^+$  case, the oscillation amplitude of the order parameters in long-time regime decreases with increasing system time. The average of the order parameters in the long-time regime are close to each other, which is consistent with the diagonal ensemble [2,83]. In the  $t_q = 8.0$ case, the main qualitative features (e.g., oscillation amplitude and frequency) obtained with 14 sites can be reproduced by a 10-site system, except for a small quantitative difference. With the two studied cases, we conclude that the results obtained with a 10-site system are indicative of the behavior in the thermodynamic limit of large system sizes.

<sup>[1]</sup> M. Kollar and M. Eckstein, Phys. Rev. A 78, 013626 (2008).

<sup>[2]</sup> M. Rigol, V. Dunjko, and M. Olshanii, Nature (London) 452, 854 (2008).

<sup>[3]</sup> H. Aoki, N. Tsuji, M. Eckstein, M. Kollar, T. Oka, and P. Werner, Rev. Mod. Phys. 86, 779 (2014).

<sup>[4]</sup> A. Eckardt, Rev. Mod. Phys. 89, 011004 (2017).

- [5] A. de la Torre, D. M. Kennes, M. Claassen, S. Gerber, J. W. McIver, and M. A. Sentef, Rev. Mod. Phys. 93, 041002 (2021).
- [6] J. H. Mentink, K. Balzer, and M. Eckstein, Nat. Commun. 6, 6708 (2015).
- [7] M. Bukov, M. Kolodrubetz, and A. Polkovnikov, Phys. Rev. Lett. 116, 125301 (2016).
- [8] M. Puviani and F. Manghi, Phys. Rev. B 94, 161111(R) (2016).
- [9] A. Ono and S. Ishihara, Phys. Rev. Lett. 119, 207202 (2017).
- [10] M. Claassen, H.-C. Jiang, B. Moritz, and T. P. Devereaux, Nat. Commun. 8, 1192 (2017).
- [11] J. Liu, K. Hejazi, and L. Balents, Phys. Rev. Lett. 121, 107201 (2018).
- [12] D. M. Kennes, A. de la Torre, A. Ron, D. Hsieh, and A. J. Millis, Phys. Rev. Lett. 120, 127601 (2018).
- [13] K. Seetharam, P. Titum, M. Kolodrubetz, and G. Refael, Phys. Rev. B 97, 014311 (2018).
- [14] M. Messer, K. Sandholzer, F. Görg, J. Minguzzi, R. Desbuquois, and T. Esslinger, Phys. Rev. Lett. 121, 233603 (2018).
- [15] K. Sandholzer, Y. Murakami, F. Görg, J. Minguzzi, M. Messer, R. Desbuquois, M. Eckstein, P. Werner, and T. Esslinger, Phys. Rev. Lett. 123, 193602 (2019).
- [16] T. Kaneko, T. Shirakawa, S. Sorella, and S. Yunoki, Phys. Rev. Lett. 122, 077002 (2019).
- [17] M. Vogl, P. Laurell, A. D. Barr, and G. A. Fiete, Phys. Rev. X 9, 021037 (2019).
- [18] M. Kiffner, J. R. Coulthard, F. Schlawin, A. Ardavan, and D. Jaksch, Phys. Rev. B 99, 085116 (2019).
- [19] S. Chaudhary, D. Hsieh, and G. Refael, Phys. Rev. B **100**, 220403(R) (2019).
- [20] T. Oka and S. Kitamura, Annu. Rev. Condens. Matter Phys. **10**, 387 (2019).
- [21] J. Li and M. Eckstein, Phys. Rev. Lett. 125, 217402 (2020).
- [22] H. Gao, J. R. Coulthard, D. Jaksch, and J. Mur-Petit, Phys. Rev. Lett. 125, 195301 (2020).
- [23] V. L. Quito and R. Flint, Phys. Rev. Lett. 126, 177201 (2021).
- [24] N. Arakawa and K. Yonemitsu, Phys. Rev. B 103, L100408 (2021).
- [25] U. Kumar and S.-Z. Lin, Phys. Rev. B 103, 064508 (2021).
- [26] L. Stojchevska, I. Vaskivskyi, T. Mertelj, P. Kusar, D. Svetin, S. Brazovskii, and D. Mihailovic, Science **344**, 177 (2014).
- [27] N. Tsuji, T. Oka, P. Werner, and H. Aoki, Phys. Rev. Lett. 106, 236401 (2011).
- [28] J. K. Freericks, V. M. Turkowski, and V. Zlatić, Phys. Rev. Lett. 97, 266408 (2006).
- [29] J. K. Freericks, Phys. Rev. B 77, 075109 (2008).
- [30] M. Eckstein and P. Werner, Phys. Rev. Lett. 107, 186406 (2011).
- [31] D. Fausti, R. I. Tobey, N. Dean, S. Kaiser, A. Dienst, M. C. Hoffmann, S. Pyon, T. Takayama, H. Takagi, and A. Cavalleri, Science 331, 189 (2011).
- [32] S. Kitamura and H. Aoki, Phys. Rev. B 94, 174503 (2016).
- [33] L. D'Alessio and M. Rigol, Phys. Rev. X 4, 041048 (2014).
- [34] A. Lazarides, A. Das, and R. Moessner, Phys. Rev. Lett. 112, 150401 (2014).
- [35] A. Lazarides, A. Das, and R. Moessner, Phys. Rev. E 90, 012110 (2014).
- [36] P. Ponte, Z. Papić, F. Huveneers, and D. A. Abanin, Phys. Rev. Lett. 114, 140401 (2015).
- [37] A. Lazarides, A. Das, and R. Moessner, Phys. Rev. Lett. **115**, 030402 (2015).

- [38] K. I. Seetharam, C.-E. Bardyn, N. H. Lindner, M. S. Rudner, and G. Refael, Phys. Rev. X 5, 041050 (2015).
- [39] T. Shirai, T. Mori, and S. Miyashita, Phys. Rev. E 91, 030101(R) (2015).
- [40] H. Fotso, K. Mikelsons, and J. K. Freericks, Sci. Rep. 4, 4699 (2015).
- [41] A. V. Joura, J. K. Freericks, and A. I. Lichtenstein, Phys. Rev. B 91, 245153 (2015).
- [42] H. F. Fotso and J. K. Freericks, Front. Phys. 8, 324 (2020).
- [43] D. A. Abanin, W. De Roeck, and F. Huveneers, Phys. Rev. Lett. 115, 256803 (2015).
- [44] D. A. Abanin, W. De Roeck, W. W. Ho, and F. Huveneers, Phys. Rev. B 95, 014112 (2017).
- [45] K. Mallayya, M. Rigol, and W. De Roeck, Phys. Rev. X 9, 021027 (2019).
- [46] K. Mallayya and M. Rigol, Phys. Rev. Lett. 123, 240603 (2019).
- [47] K. Mallayya and M. Rigol, Phys. Rev. B 104, 184302 (2021).
- [48] M. Rigol, V. Dunjko, V. Yurovsky, and M. Olshanii, Phys. Rev. Lett. 98, 050405 (2007).
- [49] M. A. Cazalilla, Phys. Rev. Lett. 97, 156403 (2006).
- [50] A. Iucci and M. A. Cazalilla, Phys. Rev. A 80, 063619 (2009).
- [51] M. Rigol, Phys. Rev. A 80, 053607 (2009).
- [52] G. Roux, Phys. Rev. A 79, 021608(R) (2009).
- [53] M. Eckstein, M. Kollar, and P. Werner, Phys. Rev. Lett. 103, 056403 (2009).
- [54] M. Eckstein, M. Kollar, and P. Werner, Phys. Rev. B 81, 115131 (2010).
- [55] L. Du, L. Huang, and G. A. Fiete, Phys. Rev. B 96, 165151 (2017).
- [56] L. Du and G. A. Fiete, Phys. Rev. B 97, 085152 (2018).
- [57] S. R. Manmana, V. Meden, R. M. Noack, and K. Schönhammer, Phys. Rev. B 70, 155115 (2004).
- [58] A. Samanta and R. Sensarma, Phys. Rev. B 94, 224517 (2016).
- [59] M. Sekania, D. Baeriswyl, L. Jibuti, and G. I. Japaridze, Phys. Rev. B 96, 035116 (2017).
- [60] N. T. H. Yen, L. D. Anh, H. A. Tuan, N. T. Thang, and N. T. Huong, Commun. Phys. 29, 305 (2019).
- [61] D. C. Padilla-González, R. Franco, and J. Silva-Valencia, arXiv:2109.08716.
- [62] A. Chattopadhyay, Phys. Rev. B 103, 045125 (2021).
- [63] P. Calabrese and J. Cardy, J. Stat. Mech.: Theory Exp. (2005) P04010.
- [64] P. Calabrese and J. Cardy, Phys. Rev. Lett. 96, 136801 (2006).
- [65] V. Eisler and I. Peschel, J. Stat. Mech.: Theory Exp. (2007) P06005.
- [66] P. Calabrese and J. Cardy, J. Stat. Mech.: Theory Exp. (2007) P10004.
- [67] B. Kloss, Y. B. Lev, and D. Reichman, Phys. Rev. B 97, 024307 (2018)
- [68] S. Goto and I. Danshita, Phys. Rev. B 99, 054307 (2019).
- [69] M. A. Cazalilla, A. F. Ho, and T. Giamarchi, Phys. Rev. Lett. 95, 226402 (2005).
- [70] E. Wille, F. M. Spiegelhalder, G. Kerner, D. Naik, A. Trenkwalder, G. Hendl, F. Schreck, R. Grimm, T. G. Tiecke, J. T. M. Walraven, S. J. J. M. F. Kokkelmans, E. Tiesinga, and P. S. Julienne, Phys. Rev. Lett. 100, 053201 (2008).
- [71] T. Esslinger, Annu. Rev. Condens. Matter Phys. 1, 129 (2010).
- [72] H. P. Büchler, Phys. Rev. Lett. 104, 090402 (2010).
- [73] T. J. Park and J. C. Light, J. Chem. Phys. 85, 5870 (1986).

- [74] N. Mohankumar and S. M. Auerbach, Comput. Phys. Commun. 175, 473 (2006).
- [75] M. Balzer, N. Gdaniec, and M. Potthoff, J. Phys.: Condens. Matter 24, 035603 (2012).
- [76] H. Lu, S. Sota, H. Matsueda, J. Bonča, and T. Tohyama, Phys. Rev. Lett. 109, 197401 (2012).
- [77] M. Innerberger, P. Worm, P. Prauhart, and A. Kauch, Eur. Phys. J. Plus 135, 922 (2020).
- [78] C. Moler and C. Van Loan, SIAM Rev. 45, 3 (2003).

- [79] J. Jaklič and P. Prelovšek, Phys. Rev. B 49, 5065 (1994).
- [80] J. Li and H.-Q. Lin, Chin. Phys. B 31, 050203 (2022).
- [81] I. Grusha, M. Menteshashvili, and G. I. Japaridze, Int. J. Mod. Phys. B **30**, 1550260 (2016).
- [82] S. Trotzky, P. Cheinet, S. Folling, M. Feld, U. Schnorrberger, A. M. Rey, A. Polkovnikov, E. A. Demler, M. D. Lukin, and I. Bloch, Science 319, 295 (2008).
- [83] C. Peng and X. Cui, Phys. Rev. B **106**, 214311 (2022).